Long-term efficacy, safety and biocompatibility of a novel sirolimus eluting iron bioresorbable scaffold in a porcine model

Ya-Nan Gao [a,1], Hong-Tao Yang [e,1], Zi-Feng Qiu [h,1], Feng Qi [g], Qian-Hong Lu [b], Jian-Feng Zheng [i], Zi-Wei Xi [j], Xin Wang [c], Li Li [d], Gui Zhang [f], De-Yuan Zhang [f], Yu-Die Lu [f], Hai-Ping Qi [f], Hong Qiu [a,*], Run-Lin Gao [b,**], Yu-Feng Zheng [k,***]

[a] Department of Cardio-Metabolic Medicine Center, Fuwai Hospital, National Center for Cardiovascular Diseases, Chinese Academy of Medical Sciences and Peking Union Medical College, Beijing, China
[b] Department of Cardiology, Coronary Artery Disease Center, Fuwai Hospital, National Center for Cardiovascular Diseases, Chinese Academy of Medical Sciences and Peking Union Medical College, Beijing, China
[c] Beijing Key Laboratory of Pre-clinical Research and Evaluation for Cardiovascular Implant Materials, Animal Experimental Center, Fuwai Hospital, National Center for Cardiovascular Diseases, Chinese Academy of Medical Sciences and Peking Union Medical College, Beijing, China
[d] Department of Pathology, Fuwai Hospital, National Center for Cardiovascular Diseases, Chinese Academy of Medical Sciences and Peking Union Medical College, Beijing, China
[e] School of Engineering Medicine, Beihang University, Beijing, China
[f] R&D Center, Biotyx Medical (Shenzhen) Co. Ltd., Shenzhen, China
[g] Department of Cardiology, Fuwai Yunnan Hospital, Chinese Academy of Medical Sciences, Affiliated Cardiovascular Hospital of Kunming Medical University, Kunming, China
[h] Peking University Health Science Center, Beijing, China
[i] Department of Cardiology, Beijing Tsinghua Changgung Hospital, Beijing, China
[j] Department of Cardiology, Beijing Anzhen Hospital, Capital Medical University, Beijing Institute of Heart Lung and Blood Vessel Diseases, Beijing, China
[k] School of Materials Science and Engineering, Peking University, Beijing, China

ARTICLE INFO

ABSTRACT

Iron is considered as an attractive alternative material for bioresorbable scaffolds (BRS). The sirolimus eluting iron bioresorbable scaffold (IBS), developed by Biotyx Medical (Shenzhen, China), is the only iron-based BRS with an ultrathin-wall design. The study aims to investigate the long-term efficacy, safety, biocompatibility, and lumen changes during the biodegradation process of the IBS in a porcine model. A total of 90 IBSs and 70 cobalt-chromium everolimus eluting stents (EES) were randomly implanted into nonatherosclerotic coronary artery of healthy mini swine. The multimodality assessments including coronary angiography, optical coherence tomography, micro-computed tomography, magnetic resonance imaging, real-time polymerase chain reaction (PCR), and histopathological evaluations, were performed at different time points. There was no statistical difference in area stenosis between IBS group and EES group at 6 months, 1year, 2 years and 5 years. Although the scaffolded vessels narrowed at 9 months, expansive remodeling with increased mean lumen area was found at 3 and 5 years. The IBS struts remained intact at 6 months, and the corrosion was detectable at 9 months. At 5 years, the iron struts were completely degraded and absorbed in situ, without in-scaffold restenosis or thrombosis, lumen collapse, aneurysm formation, and chronic inflammation. No local or systemic toxicity and abnormal histopathologic manifestation were found in all experiments. Results from real-time PCR indicated that no sign of iron overload was reported in scaffolded segments. Therefore, the IBS shows comparable efficacy, safety, and

biocompatibility with EES, and late lumen enlargement is considered as a unique feature in the IBS-implanted vessels.

1. Introduction

The introduction of bioresorbable scaffold (BRS) is believed to mark the fourth revolution in interventional cardiology. As a novel approach for the treatment of coronary artery disease (CAD), BRS addresses some theoretical limitations of drug eluting stent (DES), including permanent caging vessel, limitation of vasomotion, adaptive vascular remodeling, and very late stent thrombosis [1–3]. The most representative BRS devices are poly-L-lactic acid (PLLA) based Absorb Bioresorbable Vascular Scaffold (Absorb BVS, Abbott Vascular, California, USA) and magnesium-based DREAMS 2G (marked as Magmaris, Biotronik AG, Bülach, Switzerland). Results from the first-in-man ABSORB Cohort A trial revealed a low rate of adverse events at 1 year, accompanied by restored vasomotion and late lumen enlargement at 2 years. Unfortunately, the Absorb BVS withdrawal from markets owing to the increased risk of target lesion revascularization during long-term follow-up period [4,5]. The experience with BRS technology using PLLA was limited by thick-strut and increased rate of scaffold thrombosis [4]. Notably, strut thickness is one of the principal features thought to be the mechanism behind device-related thrombosis [6]. Clinical data for Magmaris showed a promising result up to 24 months, indicated by low rate of target lesion failure [7]. However, the minimal lumen area of scaffolded vessels exhibited a decreasing trend between 6 months and 12 months [8]. The strut thickness of Magmaris is similar to that of Absorb BVS, and the comparison between Magmaris and second-generation DES also demonstrated higher late lumen loss and increased rate of target lesion revascularization in Magmaris group [9].

Pure iron presents mechanical strength inferior to 316L stainless steel and cobalt-chromium alloy. Iron-based scaffolds are emerging as promising technology, benefited by a polymer coating [10–15]. The sirolimus eluting iron bioresorbable scaffold (IBS), developed by Biotyx Medical (Shenzhen, China), uses iron as a material. It holds the distinction of being the only fully degradable scaffold with a thin-wall design (70 μm in total). The strut thickness of IBS is much lower than that of other BRS devices. Initial results from preclinical study in a porcine model demonstrated that the IBS exhibited comparable operability, efficacy, and safety to the cobalt-chromium everolimus eluting stent (EES) (marked as XIENCE PRIME™, Abbott) within 6 months [16]. However, the long-term performance of IBS remains unknown. Herein, the present study aims to firstly report the 5-year experimental data on the comparison of the efficacy, safety, and biocompatibility between IBS and EES, encompassing to explore the lumen changes of the IBS-implanted vessels during the biodegradation process.

2. Methods

2.1. Study device

The design of IBS has been reported previously (Fig. S1) [16,17]. The novel IBS consists of an ultrathin nitrided iron (Fe-0.05%N) backbone (50~55 μm), zinc sacrificial layer (600 nm) and poly-D, L-lactic acid (PDLLA) coating with sirolimus. Advantages for IBS include: (1) the thinnest strut; (2) excellent operation performance; (3) reasonable corrosion rate; (4) good visibility; (5) high drug utilization; and (6) rapid endothelialization [18]. The devices were available to operators in specifications $\Phi 3.0 \times 15$ mm and $\Phi 2.75 \times 15$ mm in the present study. The current leading device, second-generation cobalt-chromium EES, showed favorable efficacy and safety in randomized trials, and was widely chosen as comparator for device performance in previous studies [19–21]. It consists of a thin-wall strut platform (81 μm) coated with everolimus (1.0 μg/mm^2), which is incorporated into a biocompatible

polymer [22]. The stent strut thickness is 96 μm in total. The control group was implanted with the state-of-art EES with the same specification to the IBS.

2.2. Animal models

The study was conducted by using 80 healthy, 8–9 months old, weight ranging 25 kg–35 kg, Bama mini swine (Da Shuo Biotechnology Co., Ltd, Cheng Du, China). The experimental animals were randomly assigned to Group A (IBS group, N = 45) and Group B (EES group, N = 35), and underwent in vivo and ex vivo evaluations according to the study protocol (Supplementary Table S1). The mini swine in group A were divided into Group A$_1$ (N = 40) and Group A$_2$ (N = 5 + 3) thereafter, and there were three experimental animals involved in Group A$_1$ and Group A$_2$ simultaneously. The comparison of efficacy, safety, and biocompatibility were conducted between Group A$_1$ and Group B at 7 days, 14 days, 28 days, 90 days, 6 months, 1 year, 2 years, and 5 years after device implantation, and the mid-term results within 6 months were reported previously [16]. The specific grouping, follow-up times, and evaluation methods were described in Table 1. A serial clinical and imaging evaluation were performed in Group A$_2$ at baseline, 9-month, 3-year, and 5-year follow-up to observe the biodegradation process and lumen changes of the IBS. The sample size and examination flow-chart of Group A$_2$ were shown in Fig. 1. Additionally, the specific information on grouping, implanted device, and follow-up time points of all experiments were shown in the Supplementary Table S2. This study was approved by the Institutional Animal Ethics Committee of Fuwai Hospital.

2.3. Device implantation

A loading dose of 300 mg aspirin and 300 mg clopidogrel was prescribed orally in the experiments within 24h prior to device implantation. Detailed information on coronary angiography and stent/scaffold implantation were described previously [16,23]. Briefly, all mini swine were injected intramuscularly with pentobarbital sodium (15–18 mg/kg) and thiolazine hydrochloride (10–12 mg/kg) for anesthesia induction, and the anesthesia was maintained by intravenous injection of propofol injection (2–8 mg/kg). Coronary angiography was performed trans femoral artery approach. Heparin (200IU/kg) was administrated through catheter to maintain an activated coagulation time of >300s during the procedure. Under support of intubation and mechanical ventilation, each experimental animal was implanted with the same material in left anterior descending artery (left circumflex artery as an alternative) and right coronary artery. The scaffold and stent balloons were inflated with a 1.1:1 to 1.2:1 ratio of scaffold to artery or stent to artery diameter. Amoxicillin (1–2 g/day) was given intravenously to the animals for 3 days after device implantation. Meanwhile, dual antiplatelet therapy including aspirin (100 mg/d) and clopidogrel (75 mg/d) was taken orally for 3 months, and then aspirin 100 mg per day was maintained through the entire follow-up period until the experiments were sacrificed.

2.4. In-vivo imaging assessments

The magnetic resonance safety and compatibility of IBS has been demonstrated [24]. Three mini swine in Group A$_2$ underwent cardiac magnetic resonance imaging (MRI) (MAGNETOM Lumina, Siemens) examination at 9 months and 5 years after scaffold implantation to investigate myocardial structure and function, and degradation profiles during the vessel healing. The intravascular images were obtained from

coronary angiography (Allura Xper FD20, Philips Medical Systems, Best, the Netherlands) and optical coherence tomography (OCT) (C7 XR, Light Lab Imaging, St. Jude Medical, Westford, Massachusetts). An OCT catheter was positioned in the distal end of the stent/scaffold segment with a 0.014-inch guidewire through a 6F guiding catheter. The OCT images were acquired at automatic pull-back speed of 20 mm/s. The region of beginning 2 mm distal to and extending 2 mm proximal to the stented/scaffolded segment was examined and analyzed at 10 frames (2 mm) intervals. OCT measurements including lumen diameter, lumen area, stent/scaffold diameter, stent/scaffold area, and neointima thickness were employed to characterize the long-term changes of intracoronary lumen. The lumen area and stent/scaffold area were measured by a computer-based contour detection program with manual calibration. Area stenosis was calculated as: (mean lumen area at baseline – mean lumen area at follow-up)/mean lumen area at baseline. The in-stent/scaffold restenosis was defined as the value of area stenosis ≥ 50 %. Diameter stenosis was defined as: (mean lumen diameter at baseline – mean lumen diameter at follow-up)/mean lumen diameter at baseline. For semi-quantitative analyses of strut biodegradation, iron struts in each crossing-section were classified and counted according to the morphology. The radial height of the deformed strut (arched highlight area with shadowing behind in OCT image was measured to identify the iron degradation degree, and weight loss (WL_{OCT}) of iron was calculated by accumulating $N_n d_n$ (N: the total strut number; d: degradation degree). The specific description of this formula was reported by Gao et al., and this approach was confirmed to be consistent with the widely-used weighing method [25].

2.5. Ex-vivo assessments

At the pre-set time point, the animals were sacrificed by injection of potassium chloride after in vivo observation. The animals underwent autopsy by gross observation and histopathological evaluation. The heart and other main organs including liver, spleen, lung, and kidney, were rapidly harvested according to the methods reported previously [16,23]. The blank vessels and samples from the five main organs were immediately immersed in 4 % formaldehyde solution for fixation, then underwent dehydration by a fully enclosed tissue processor (ASP200 S, Leica), vitrification with xylol, and paraffin embedding. After that, the 4-5μm paraffin-embedded sections were prepared by using a rotary microtome (RM2235, Leica), followed by xylene dewaxing, gradient rehydration, neutralization in a 0.05M sodium hydroxide solution, rinsing and hematoxylin eosin (HE) staining. The optical microscope (OM) (VHX-970F, Keyence) was employed for histomorphology observation.

The scaffolded and stented vessel including proximal and distal edges were carefully dissected from the epicardial surface of heart and immersed in 4 % formaldehyde solution. Only vessels implanted with the IBS underwent micro-computed tomography (Micro-CT) (Skyscan 1172, Bruker, Kontich, Belgium) before cutting off to examine the morphology and corrosion condition of the iron struts. The artificial intelligence filtering technology was employed to acquire the integral structure of iron struts, and the value of $WL_{micro-CT}$ was calculated by the supporting software. After that, the scaffolded and stented vessels were cut into proximal, middle, and distal segments as illustrated previously [16]. Then the vessel segments were prepared by conventional fixing, dehydration, methyl methacrylate embedding, and sectioning, and the HE staining was conducted to observe the histomorphology, inflammation and fibrin deposition [26]. The HE staining process was in accordance with the conventional methodologies.

Additionally, the proximal, middle, distal sections of the IBS-implanted vessels were divided into scaffolded segments and blank segments. The quantitative real-time polymerase chain reaction (PCR) was performed in these specimens to observe recovery of endothelial cell physiological function, inflammation response, and iron metabolism. The RNeasy Mini Kit (Qiagen) was acquired to collect cellular ribonucleic acid (RNA), and the M-MLV reverse transcription kit (Promega) was used for reverse transcription. The process was normalized to glyceraldehyde-3-phosphate dehydrogenase (GAPDH). The GAPDH forward primer and reverse primer were 50-ACAGCAACAGGGTGGTG-GAC-30 and 50-TTTGAGGGTGCAGCGAACTT-30, respectively. The primers and probes used by real-time PCR were commercial products (Sangon Biotech, China), and detailed information were described in the Supplementary Table S3. The comparative Ct method was adopted to determine relative mRNA quantities. The expression levels of ferritin, interleukin (IL)-1β, IL-4, IL-10, tumor necrosis factor (TNF)-α, endothelial nitric oxide synthase (eNOS), heme oxygenase(HO)-1, nicotinamide adenine dinucleotide phosphate (NADPH), and superoxide dismutase (SOD)-1 were compared between the scaffolded segments and blank segments.

2.6. Statistical analysis

Continuous variables were described as mean $\pm$ standard deviation (SD) or median and interquartile ranges (IQR) and compared using Student's t-test or Mann-Whitney U test as appropriate. Test of normality by Shapiro Wilk test was denoted for non-parametric/parametric discrimination. Categorical variables were summarized by frequency and percentage and analyzed by Pearson chi-square or Fisher's exact test as appropriate. All tests were two sides, and a value of $P < 0.05$ was considered statistically significant. Statistical analysis was done with SPSS version 24.0 software (IBM, Inc., Chicago, IL, USA).

Table 1
Groups, follow-up times, and evaluation methods.

Follow-up	Group A$_1$		Group B		Methods
	Mini swine (N = 40)	Coronary arteries (n = 80)	Mini swine (N = 35)	Coronary arteries (n = 70)	
7 days*	3	6	3	6	D
14 days*	3	6	3	6	D
28 days*	8	16	8	16	A, B, C, D, E, F
90 days*	5	10	5	10	A, B, C, E
6 months*	5	10	5	10	A, B, C, E
1 year	5	10	5	10	A, B, C, E
1.5 years	3	6	/	/	A, B, C, E
2 years	5	10	3	6	A, B, C, E
5 years	3#	6	3	6	A, B, C, E

Note: The Group A$_1$ and Group B were implanted with the IBS and EES, respectively. A = coronary angiography; B = optical coherence tomography; C = Micro-–computed tomography; D = scanning electron microscopy; E = histopathology; F = immunohistochemistry; N = number of mini swine; n = number of coronary arteries; EES = everolimus eluting stents; IBS = sirolimus eluting iron bioresorbable coronary scaffold; * = initial results within 6 months were reported previously; # = These mini swine were selected to constitute Group A$_2$ and were consecutively followed up at each predefined timepoint.

3. Results

3.1. Efficacy

All scaffolded and stented vessels remained patent during the investigation period by coronary angiography and OCT examination. The typical images of coronary angiography at different follow-up time points were shown in the Supplementary Fig. S2. Manifestation on OCT and comparison of area stenosis between Group A_1 and Group B at each time point were presented in Fig. 2. Correspondingly, the lumen contour was smooth during 2-year follow-up period, and complete neointimal coverage of scaffold/stent was observed, without struts protrude, premature fracture, recoil, or collapse. No fibrous plaque, calcific plaque and fibroatheroma were found within the neointima. There were no statistical differences in area stenosis between Group A_1 and Group B at 6 months (27.0 ± 9.0 % vs. 31.0 ± 16.0 %), 1 year (30.8 ± 5.2 % vs. 27.4 ± 8.9 %), 2 years (31.2 ± 11.9 % vs. 29.2 ± 18.7 %), or even 5 years (26.4 ± 12.7 % vs. 25.0 ± 14.0 %) (all $P > 0.05$). Regarding on area stenosis of the IBS-implanted vessels at different time points, no significant differences were found between 6 months and 1 year (27.0 ± 9.0 % vs. 30.8 ± 5.2 %, $P = 0.270$), 1 year and 2 years (30.8 ± 5.2 % vs. 31.2 ± 11.9 %, $P = 0.945$), 2 years and 5 years (31.2 ± 11.9 % vs. 26.4 ± 12.7 %, $P = 0.906$), either. In addition, the percentages of area stenosis for both groups at each follow-up time point were lower than 50 %, indicating that no in-stent/scaffold restenosis happened. The results demonstrated that the IBS had comparable efficacy with the EES during the long-term investigation. The comparison of OCT measurements between the two groups at different times was summarized in the Supplementary Table S4. Additionally, the change in mean scaffold area over time was illustrated in Table 2. The values of mean scaffold area at 9 months and 3 years were comparable (6.13 ± 1.95 mm² vs. 6.29 ± 1.24 mm², $P = 0.672$), indicating that the IBS did not recoil or collapse and could provide sufficient scaffolding to vessel during the 3-year follow-up period.

3.2. Lumen changes

The experimental animals in Group A_2 underwent a serial of OCT examination at baseline, 9 months, 3 years, and 5 years to acquire the sequential changes in mean lumen area and strut degradation. As shown in Fig. 3 and Table 2, significant luminal narrowing was found during mid-term follow-up period, indicated by the mean lumen area decreasing from 6.54 ± 1.38 mm² post procedure to 3.66 ± 1.34 mm² at 9 months. Reduction in mean lumen area was considered as the consequence of neointima proliferation. As the iron struts corroded over time, the neointima became stable, and the maximum neointima thickness was not significantly differed between 9 months and 3 years (0.41 ± 0.08 mm vs. 0.37 ± 0.11 mm, $P = 0.100$). Interestingly, the mean lumen area increased (3.97 ± 1.34 mm² at 3 years; 4.66 ± 1.66 mm² at 5 years), and the area stenosis decreased (37.1 ± 12.5 % at 3 years; 26.4 ± 12.7 % at 5 years) during the long-term investigation period. Late lumen enlargement in vessels implanted with the IBS was demonstrated by significant increasing trend in mean lumen area (3.66 ± 1.34 mm² vs. 4.66 ± 1.66 mm², $P = 0.032$) and statistical decrease in area stenosis (42.3 ± 14.0 % vs. 27.1 ± 13.7 %, $P = 0.012$) between 9 months and 5 years.

Group A_2 (N=8, n=16)
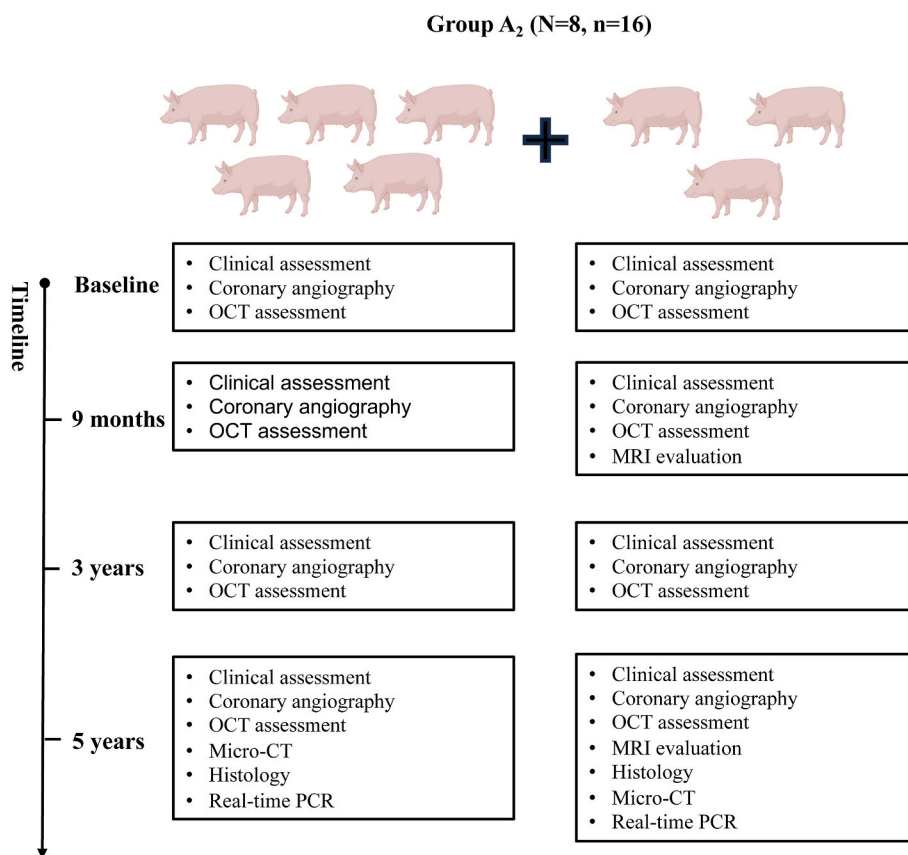
Fig. 1. Flowchart of in-vivo and ex-vivo evaluation of GroupA_2 at the predefined times. A total of 8 mini swine with 16 coronary arteries were included in Group A_2. A serial of clinical and in vivo imaging assessments was performed at baseline, 9 months, 3 years, and 5 years post procedure. The specific evaluation methods were listed. All mini swine were sacrificed and underwent ex vivo assessment at 5 years. N = number of mini swine; n = number of coronary arteries; MRI = magnetic resonance imaging; Micro-CT = micro-computed tomography; OCT = optical coherence tomography; PCR = polymerase chain reaction.
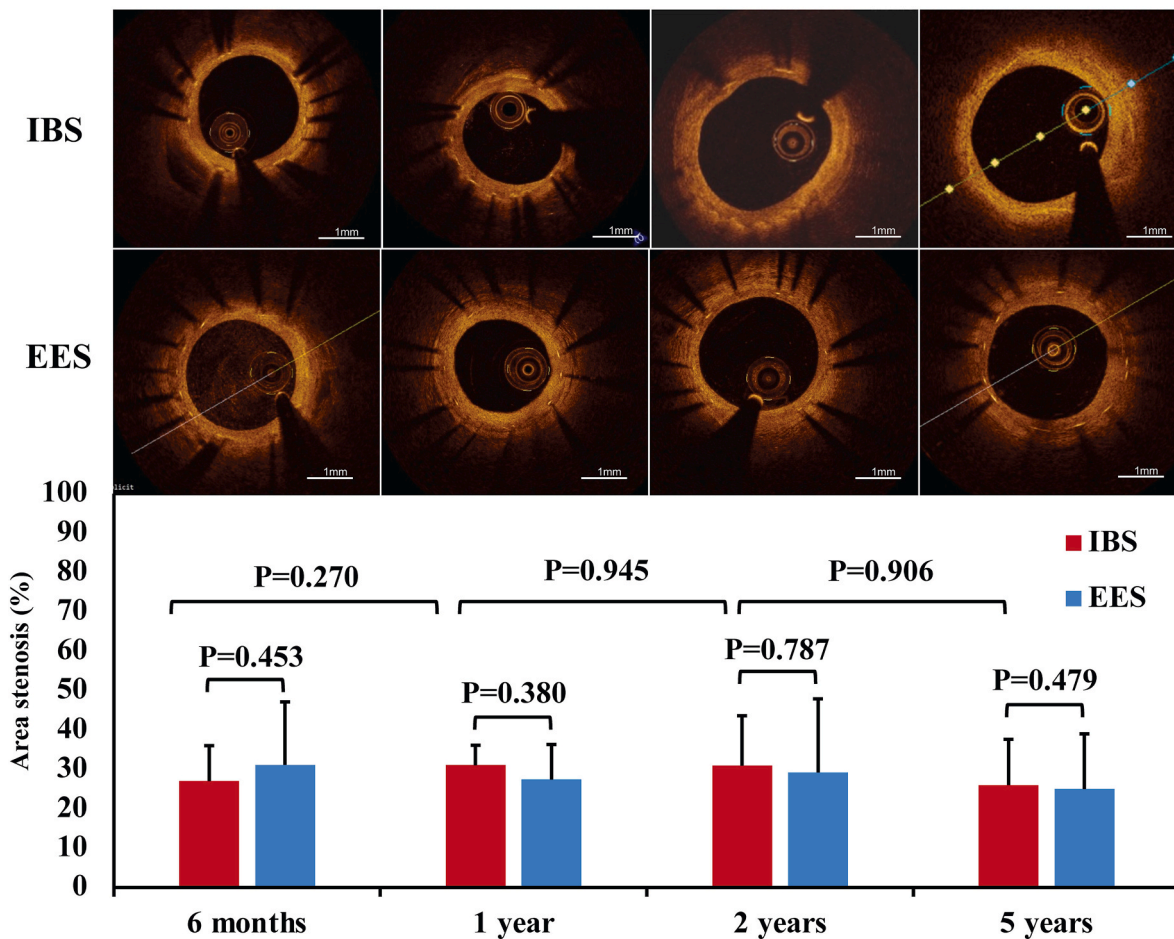
Fig. 2. Imaging manifestation and comparison of area stenosis between IBS group and EES group. (A) The cross-sectional OCT images of the IBS- and EES-implanted vessels at 6 months, 1 year, 2 years, and 5 years after procedure; (B) comparison of area stenosis via OCT measurements between the scaffolded and stented vessels at 6 months, 1 year, 2 years, and 5 years after device implantation. EES = everolimus eluting stents; IBS = sirolimus eluting iron bioresorbable coronary scaffold; OCT = optical coherence tomography.

3.3. Biodegradation process

The biodegradation process of IBS was intuitively revealed by OCT, Micro-CT, MRI, and HE staining images. As illustrated by Fig. 3, the IBS struts remained intact and were identified as thin, rich-signal, linear regions with shadowing behind post procedure. At 9 months, the iron struts were well embedded in homogenous neointima and showed sharp contours under OCT, and the value of WL_{OCT} was 14.8 ± 3.2 %. As the biodegradation process continued, the iron struts deformed and were presented as arched area with high attenuation regions under OCT, with a WL_{OCT} of 72.4 ± 16.9 % at 3 years. By the end of 5 years, the strut-like remnant was not visible on OCT images, and the value of WL_{OCT} increased to 97.2 ± 0.8 %, suggesting the complete biodegradation of the iron platform.

Regarding on the cardiac MRI images, the iron struts were detectable at 9 months. By the time of 5-year follow-up, the IBS struts were completely degraded and absorbed in situ, without any scaffold artifacts. No abnormal signal shadow or infraction lesion were found in the myocardium (Fig. S3).

The morphology and corrosion process of the iron struts at different follow-up time points were further investigated by Micro-CT and histopathology. As shown in Fig. 4, the iron struts were sharp delineated at 6 months, without obvious signs of biodegradation ($WL_{Micro-CT} = 0$ %), structure kink or lumen collapse. The IBS maintained structural integrity and the corrosion was only found at the junction of iron strut at 1 year. As the corrosion profiles diffusing to the surrounding, the iron struts

became blurred, with a $WL_{Micro-CT}$ of 21.2 ± 27.6 %. Correspondingly, the iron struts in outermost area were corroded, and the yellow-brown dots (corrosion products) were devoured by macrophages via histomorphology evaluation at 1 year, without chronic inflammation or tissue necrosis. The hemosiderin formed after the corrosion particles engulfed by macrophages (Fig. S4). More corrosion products scattered in the surrounding tissues and the iron struts were characterized as a nebulous appearance at 1.5 years and 2 years. The values of $WL_{Micro-CT}$ at 1.5 years and 2 years were 27.8 ± 12.5 %, 50.0 ± 10.6 %, respectively. Meanwhile, the histopathology observation found that area of remaining black struts decreased gradually, along with considerable corrosion products generated and eliminated by macrophages. The hemosiderin-laden macrophages moved from struts position to adventitia, accompanied by decrease of smooth muscle cells (SMCs) and collagen deposition at 2 years (Fig. S5). As the biodegradation process continued, the scaffold structure disintegrated, and the iron struts and degradation products were discernible on Micro-CT images at 5 years, with radiopaque makers left. The $WL_{Micro-CT}$ increased to 93.2 ± 6.6 %. The strut degradation assessed by Micro-CT was consistent with results from OCT evaluation. The iron struts were invisible in cross-section by gross observation. The complete biodegradation at 5 years was verified by the histomorphology exhibiting that the iron struts were degraded and absorbed in situ, the strut positions were replaced by intima tissue, and only a quantity of corrosion products were found in the vascular adventitia (Fig. 5).

Table 2
Optical coherence tomography measurements of Group A_2 at 9 months, 3 years, and 5 years.

	9 months (N = 8)	3 years (N = 8)	5 years (N = 8)	P 9 months vs. 3 years	P 3 years vs. 5 years	P 9 months vs. 5 years
Mean lumen diameter, mm	2.10 ± 0.50	2.26 ± 0.41	2.40 ± 0.43	0.237	0.440	0.069
Mean scaffold diameter, mm	2.76 ± 0.43	2.82 ± 0.27	–	0.558	–	–
Mean lumen area, mm²	3.66 ± 1.34	3.97 ± 1.34	4.66 ± 1.66	0.465	0.242	0.032*
Mean scaffold area, mm²	6.13 ± 1.95	6.29 ± 1.24	–	0.672	–	–
Mean neointima thickness, mm	0.41 ± 0.08	0.37 ± 0.11	–	0.100	–	–
Area stenosis, %	42.3 ± 14.0	37.1 ± 13.7	27.1 ± 13.7	0.277	0.051	0.012*
Diameter stenosis, %	24.7 ± 9.4	19.7 ± 9.9	15.0 ± 8.2	0.126	0.674	0.064

Note: Value are presented as mean ± standard deviation; area stenosis = (mean lumen area at baseline – mean lumen area at follow-up)/mean lumen area at baseline; diameter stenosis = (mean lumen diameter at baseline – mean lumen diameter at follow-up)/mean lumen diameter at baseline. The mini swine in Group A_2 were implanted with sirolimus eluting iron bioresorbable coronary scaffold, and the iron struts were not identifiable under OCT at 5 years, leading the mean scaffold diameter, mean scaffold area, and mean neointima thickness not available at this follow-up time point. * = statistical difference; N = number of mini swine.

3.4. Safety and biocompatibility

The scaffold structure remained obvious and intact at 3 months after implantation, and the struts were completely covered by thin-layer of endothelial cells under OCT and histopathology. The silver struts were clear and distributed around the lumen on gross observation. As the corrosion process continued, the neointima evaluated by OCT thickened at 1-year follow-up. The iron struts were surrounded by brown degradation products, and the outmost area of scaffolded vessel was infiltrated with corrosion profiles on gross observation. The local tissue exhibited slight inflammatory response to the corrosion products by. At 5 years, the iron struts were invisible on cross-section of scaffolded vessels by OCT and gross observation. Images on HE staining further demonstrated that the IBS struts were completely degraded and absorbed in situ, and the scaffolded segments recovered normal vascular structure, with clear manifestation of intima, media, and adventitia. No atrophy, loss of SMCs, or destruction of external elastic lamina was observed in vessels implanted with IBS at 5 years. No in-scaffold thrombosis or coronary artery ectasia was found within the 5-year follow-up period.

During the feeding time, all mini swine had normal living habits, weight, diet, and defecation. No myocardial infraction or adverse events related to device implantation were reported. All experimental animals survived to the pre-defined time points. At the sacrifice date, the animals were evaluated by gross observation. No evidence of epicardial hemorrhage, coronary aneurysm formation, myocardial infarction, and pathological changes were found for the five main organs (heart, liver, spleen, lung, and kidney). The histomorphology presented as normal features for the main organs at 5 years after procedure. And there was no significant difference in histopathological manifestations of the main organs between IBS group and EES group (Fig. 6).

The biocompatibility was further investigated by quatitative real-time PCR. As illustrated by Fig. 7, there was no statistical difference in the level of ferritin ($P = 0.385$), suggesting that the iron metabolism was comparable between scaffolded segments and blank segments. The restoration of endothelial function was indicated by significantly higher expression level of eNOS in scaffolded segments ($P = 0.010$). Although the levels of inflammatory biomarkers including IL-1 ($P < 0.001$), IL-10 ($P = 0.027$), HO-1 ($P = 0.002$) and TNF-α ($P = 0.050$) were higher in scaffolded segments, the value of the above indicators did not exceed twice as these of the blank segments. The results indicated that the local tissue showed a slight inflammatory response to IBS during the biodegradation process, which was consistent with the histopathology assessment. All these results provided promising evidence for long-term safety and biocompatibility of the IBS.

4. Discussion

In the present study, we firstly reported the long-term efficacy, safety, biocompatibility, and lumen changes of the ultra-thin IBS in porcine coronary artery model. The main findings of this study were as followed: (1) By the end of 5 years after device implantation, the IBS exhibited comparable efficacy with EES, and no in-stent/scaffold restenosis was found. (2) Moderate luminal narrowing existed at 9 months after IBS implantation, while the expansive remodeling was observed thereafter, verified by significant increase in mean lumen area between 9 months and 5 years. (3) The corrosion was firstly detectable at the junction of iron struts at 9 months. As the biodegradation continued, the IBS struts disintegrated gradually, and the corrosion products were devoured by macrophages during the vessel healing. (4) The IBS struts were completely degraded and absorbed in situ at 5 years, and the scaffolded segments recovered to normal vascular structure after complete biodegradation, without in-scaffold thrombosis or coronary aneurysm formation. (5) No adverse local tissue response, systemic toxicity, or abnormal manifestations were observed on gross and histopathology observation at each follow-up time point. There was not any sign of iron overload in scaffolded segments. The safety and biocompatibility of the IBS within 5-year follow-up period were favorable.

It is worth mentioning that although the mean lumen area of scaffolded vessels narrowed at 9 months, late lumen enlargement was observed thereafter. The luminal narrowing at mid-term stage was attributed to neointimal proliferation, as evidenced by OCT and histopathology. This phenomenon was also found in EES-implanted vessels in our study. Reviewing data published previously, the commentary expansive remodeling during long-term period was only found in Absorb BVS, but not in Magmaris and other BRS [1,7,27–29]. Results from ABSORB Cohort A suggested that the stability of lumen dimensions within 5-year attributed to improved clinical outcomes [30–32]. Clinical trial on magnesium based BRS also elucidated that negative remodeling became one of the main mechanisms for restenosis after scaffold implantation [33]. Furthermore, with permanent metallic frame, DES is considered as a nidus for chronic inflammation, neoatherosclerosis, and thrombosis, which contributes to increased annualized risk of very late device-related adverse events [34]. The lumen area of stented vessels, therefore, is prone to decrease over time. Late positive remodeling, on the contrary, becomes a strength of IBS over contemporary DES and other BRS (except for Absorb BRS).

The potential mechanism for positive remodeling in BRS treated vessels has not been fully elucidated. Theoretically, scaffold implantation is considered as mechanical injury to vessel, which leads to inflammation response and tissue remodeling [35]. During this period, macrophages play an important role in phagocytosis of necrotic cells or pathogens [36], and adventitial macrophages have a unique role in controlling inward vascular inflammation that couples with vascular remodeling [37]. Sustained influence of hemodynamic stress also stimulates adaptive change of vascular wall, which is characterized by an increase in luminal diameter [38,39]. As illustrated by histopathologic images from our study, Fe-laden macrophages were observed in medium
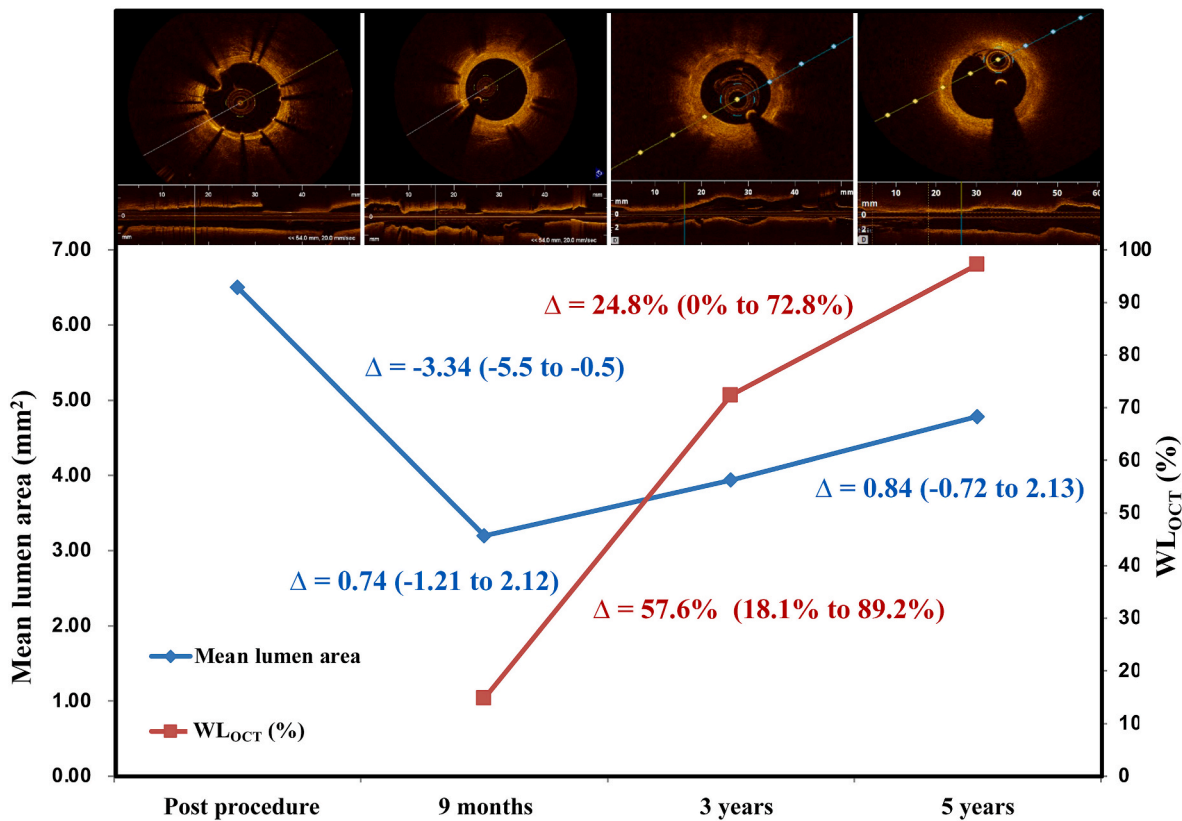
Fig. 3. Serial assessments about mean lumen area and strut degradation of the sirolimus eluting iron bioresorbable coronary scaffold.
Each representative OCT frame above the table was corresponding to the time points at the bottom. The lumen contour was smooth and free from tears, and the iron struts were clearly visible with sharp contour post procedure. At 9 months, the struts were covered by neointima, the intracoronary lumen narrowed moderately, and slight degradation was detectable. At 3 years, more iron struts deformed, and the corrosion became obvious; the mean lumen area showed an increasing trend. At 5 years, the iron struts were degraded completely and were invisible under OCT, accompanied by a sustained increase in mean lumen area. IBS = sirolimus eluting iron bioresorbable coronary scaffold; OCT = optical coherence tomography; WL = weight loss.

and adventitia in scaffolded segments during the biodegradation process, and the corrosion products were transferred to vascular adventitia by macrophages eventually. Herein, we suppose that: the solid corrosion products of iron strut are devoured by macrophages and transferred to adventitia in form of hemosiderin, and the accumulation of macrophages in adventitia promotes lumen enlargement. In addition, transient decrease of SMCs in vascular media was observed during the vessel healing. By the end of 5-year follow-up, the original media of scaffolded vessels disappeared. Instead, normal vascular structure including intima, medium and adventitia reformed, and SMCs were detectable in the newly-formed media. The apoptosis and regeneration of SMCs during the biodegradation process might also favor the phenomenon of late lumen enlargement.

The concept of BRS is attractive as the scaffolds provide temporary mechanical support for vessels until complete endothelialization and vascular remodeling are achieved. Moreover, the degradation of BRS contributes to restoration of vasomotion [40]. In this study, we visualize the complete in vivo biodegradation process of IBS in terms of comprehensive imaging methods (OCT, Micro-CT, histopathology). The IBS scaffold remained most of its structural integrity (~80 % scaffold weight) during 6–12 months after implantation. Half of the scaffold weight lost at 2-year time point, indicating a great loss of mechanical constraints on repaired vessels. At 5 years, almost no scaffold residues were observed under X-ray and OCT imaging. More importantly, the iron strut sites were replaced with newly formed tissues in histopathology. Combining the present results with previous analysis of IBS in vivo biodegradation behavior [17,41], the corrosion product and metabolism process of the IBS is presented in Fig. 8. Investigation via scanning electron microscopy, energy-dispersive spectroscopy, and

transmission electron microscopy found that the $Fe_3(PO_4)_2$ was in the outer layer of iron platform, while the γ-FeOOH was mainly infiltrated in the surrounding tissues [41]. Eventually, the corrosion products were transferred to adventitia in form of hemosiderin, then to the lymph system. Considering the absence of a benchmark for degradation frame of biodegradable scaffolds, it would certainly be wise to use clinical opinion as a reference. Regarding on the first commercial-approved biodegradable device, Absorb BVS has generated a considerable amount of clinical data. Absorb BVS is constituted by a PLLA backbone, and its first-generation can be fully degraded at 2 years [42]. To reduce the late lumen loss caused by late recoil, the second generation Absorb BVS provides persistent radial support between 6 and 12 months, and the gradual mass loss extends to approximately 3 years [43]. However, high in-scaffold thrombosis rate has been reported within the first few years before complete biodegradation [44]. The magnesium-based BRS underwent iterative progression including AMS-1, DREAMS-1G, and DREAMS-2G, with each successive generation implementing changes to improve device performance, efficacy, and safety [45].The scaffolding time of AMS-1 is only one week, and the device is completely degraded within 4 months [46]. DREAMS 1G extends the scaffolding time to 4 weeks, with a total degradation at 6 months [47]. However, DREAMS 1G exhibited a higher late lumen loss compared to DES and bioabsorbable everolimus eluting coronary stent in the first-in-man BIOSOLVE-I trial [48]. DREAMS 2G is capable to provide mechanical support up to 12 weeks and be degraded within 12 months. Clinical results from BIO-SOLVE-II indicated a more balanced degradation behavior of DREAMS 2G, as the values of scaffold area and lumen area decreased slower than DREAMS 1G [49]. The improvement of next generation DREAMS 3G exhibits a longer targeted scaffolding time of at least 12 weeks and
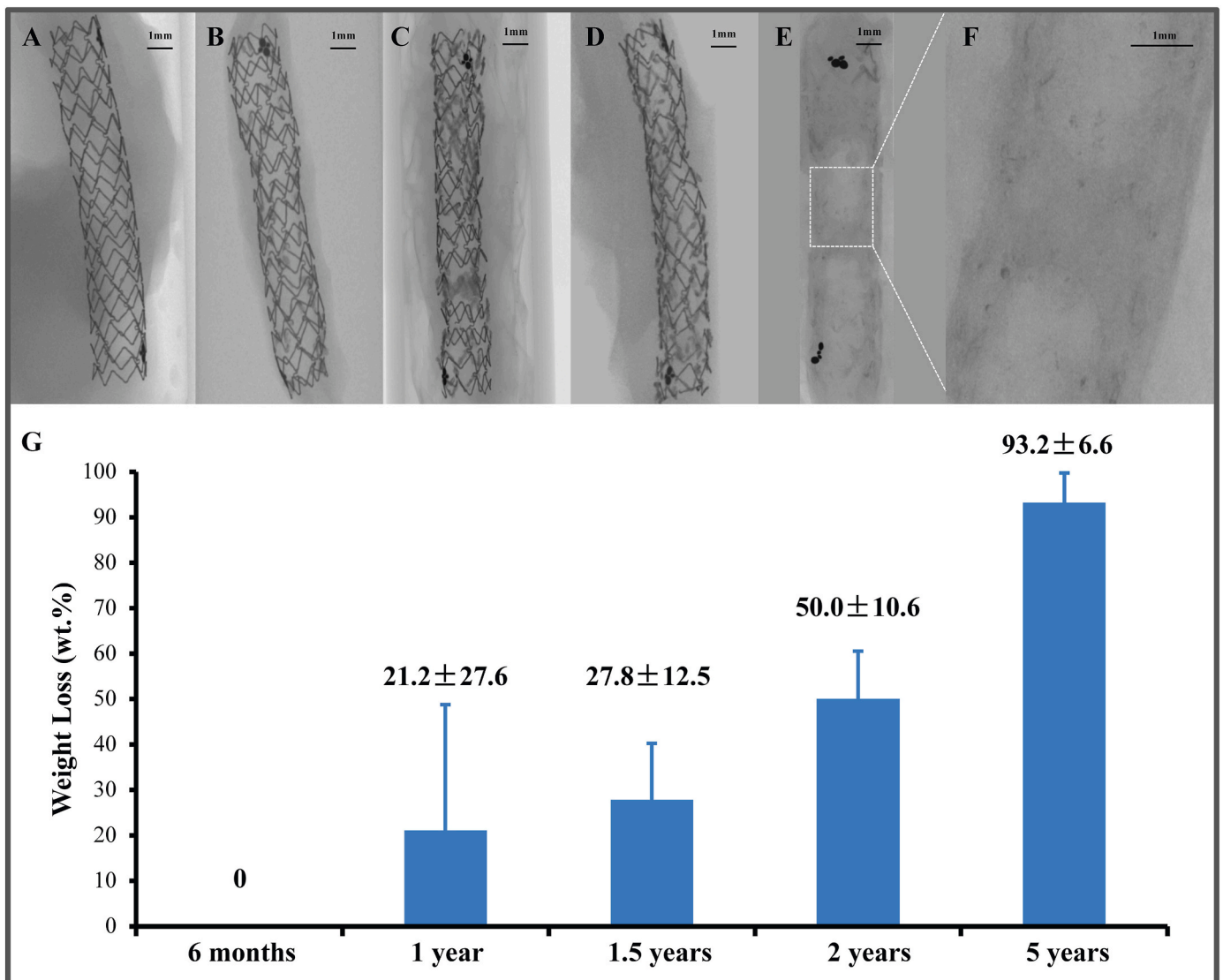
Fig. 4. Micro–computed tomographic images and weight loss of the sirolimus-eluting iron bioresorbable coronary scaffold.
(A~F) listed the typical micro–computed tomographic images of the scaffold at (A) 6 months, (B) 1 year, (C) 1.5 years, (D) 2 years, and (E) 5 years; (F) Enlargement of the rectangular area in (E); (G) illustrated the percentage of weight loss of the sirolimus-eluting iron bioresorbable coronary scaffold at each time point.

maintaining the current degradation time of 12 months [50]. Zinc-based BRS is a fast-emerging field during the last decade, and shows suitable degradable rate without complicated modification or elaborated design [51,52]. An ultrathin-strut vascular scaffold developed on high strength Zn-Li alloy shows comparable scaffold performance to clinical counterparts and favorable in vivo results in terms of area stenosis in porcine coronary arteries [53]. The volume loss of Zn-Li scaffold is similar to that of the IBS in the 12-month span, but long-term investigation is necessary to examine the full biodegradation process. Additionally, we should bear in mind that animal models have unignorable impacts on the in vivo corrosion behavior of biodegradable scaffolds.

With respect to safety and biocompatibility, iron is considered as an attractive alternative material for manufacturing BRS. Results from Hausdorf firstly reported that NOR-I, the first iron-based scaffold, could be safely implanted with low thrombogenicity and mild inflammatory response [54]. However, iron-based BRS is limited by long corrosion period, slow clearance, and residue corrosion products. The introduction of iron processed with nitriding technology and zinc sacrificial layer overcomes these inherent drawbacks. Theoretically, the degradation ingredients of IBS are iron and zinc, which are indispensable elements for human body. Iron ion will not lead excessive release of H^+ and thus a

dramatic alternation of pH, minimizing the adverse impact on local microenvironment and endothelium function restoration [28,55]. Moreover, Fe^{2+} from iron strut corrosion shows favorable effect of preventing proliferation and migration of SMCs, inhibiting the occurrence of in-scaffold restenosis [56,57]. As shown in our study, no local or system toxicity, in-scaffold restenosis or thrombosis, or abnormal histomorphology of the main organs was found. The iron metabolism was comparable between scaffold segments and blank segments. Long-term observation on safety and biocompatibility of another iron-based BRS, bioresorbable nitrided iron scaffold, revealed that the corrosion products were devoured by inflammatory cells, then transferred to vascular adventitia by macrophages, finally to the lymph system and spleen, without any systematic and local toxicity reported within 7-year follow-up period [58]. The biocompatibility of nitrided iron scaffold is favorable, and this device is the platform of IBS. In addition, the iron content in IBS with specification of 3.0 × 18 mm is theoretically negligible compared to blood's Fe overload concentration, and 3-year outcome from the first-in-man study of IBS did not report any adverse events related to IBS implantation and biodegradation [59]. Therefore, the long-term safety and biocompatibility of IBS are promising.

There are several limitations to this study. First, the porcine model
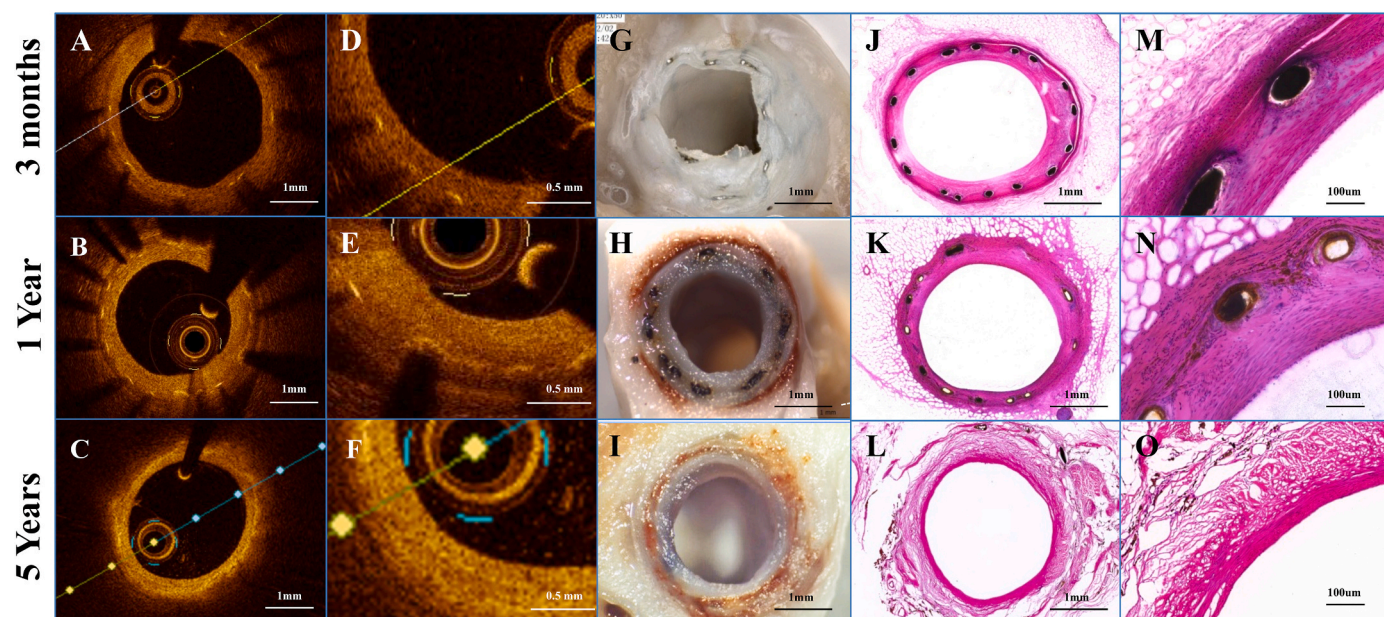
Fig. 5. In-vivo and ex-vivo assessment of the sirolimus eluting iron bioresorbable coronary scaffold. (A~F) Images via optical coherence tomography of the sirolimus eluting iron bioresorbable coronary scaffold (IBS) at (A&D) 3 months, (B&E) 1 year, and (C&F) 5 years; (D ~ F) High-power images; (G ~ I) optical micrographic images of the IBS at each time point. (J ~ O) Hematoxylin eosin staining images of the IBS at each time point. (M ~ O) High-power images.
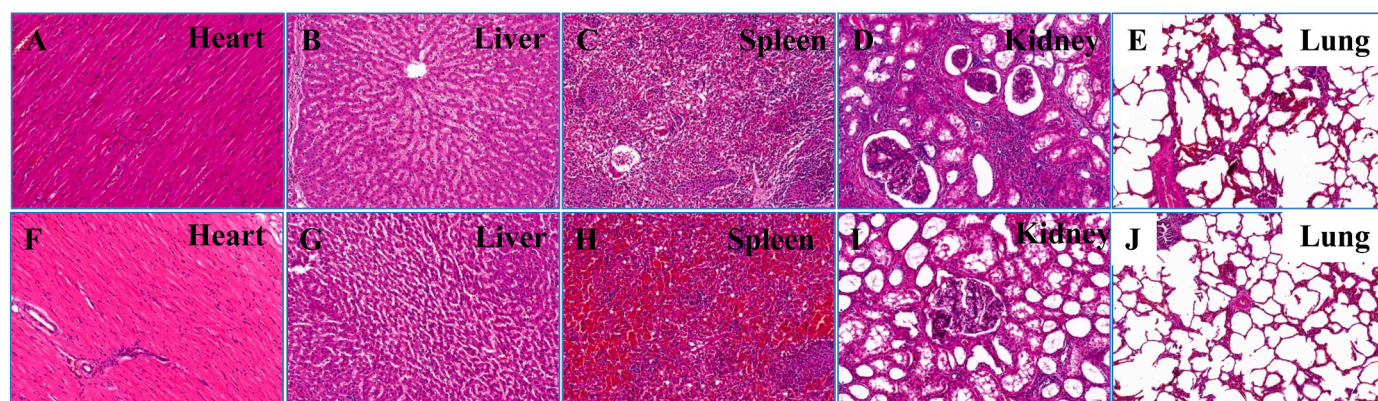
Fig. 6. Histomorphology on the main organ at 5 years after implantation of the sirolimus eluting iron bioresorbable coronary scaffolds and everolimus eluting stent.
The histopathological images by hematoxylin eosin staining of (A) heart, (B) liver, (C) spleen, (D) kidney, and (E) lung of experiments implanted with the sirolimus eluting iron bioresorbable coronary scaffolds. The histological images by hematoxylin eosin staining of (F) heart, (G) liver, (H) spleen, (I) kidney, and (J) lung of experiments implanted with the everolimus eluting stent.

could not completely represent the complex environment of human body, thereby the IBS corrosion and recycling timeline by macrophages might differ in patients. Second, by using healthy porcine model, the ability to determine the impact of IBS on lipidic, fibrotic, or calcific atherosclerotic plaques is limited. Third, the follow-up period is up to 5 years after scaffold implantation. Although the complete biodegradation is observed, there still holds necessity for very long-term investigation of iron metabolism. With convincing results provided by the present study, the clinical study with long-term follow-up period is pending.

5. Conclusions

The long-term results based on porcine model demonstrate that the novel IBS has comparable efficacy and safety to the contemporary metal-based DES up to 5 years, without any restenosis, thrombotic complications, local or systemic toxicity, or abnormal histopathologic changes; the IBS struts can be corroded and absorbed completely in situ, with good long-term biocompatibility. Remarkable advantage of the IBS is featured as late lumen enlargement during the biodegradation process, which is considered as a potential clinical benefit.

Data availability statement

H. Qiu and R.L. Gao are the guarantor of this work and has full access to all data.
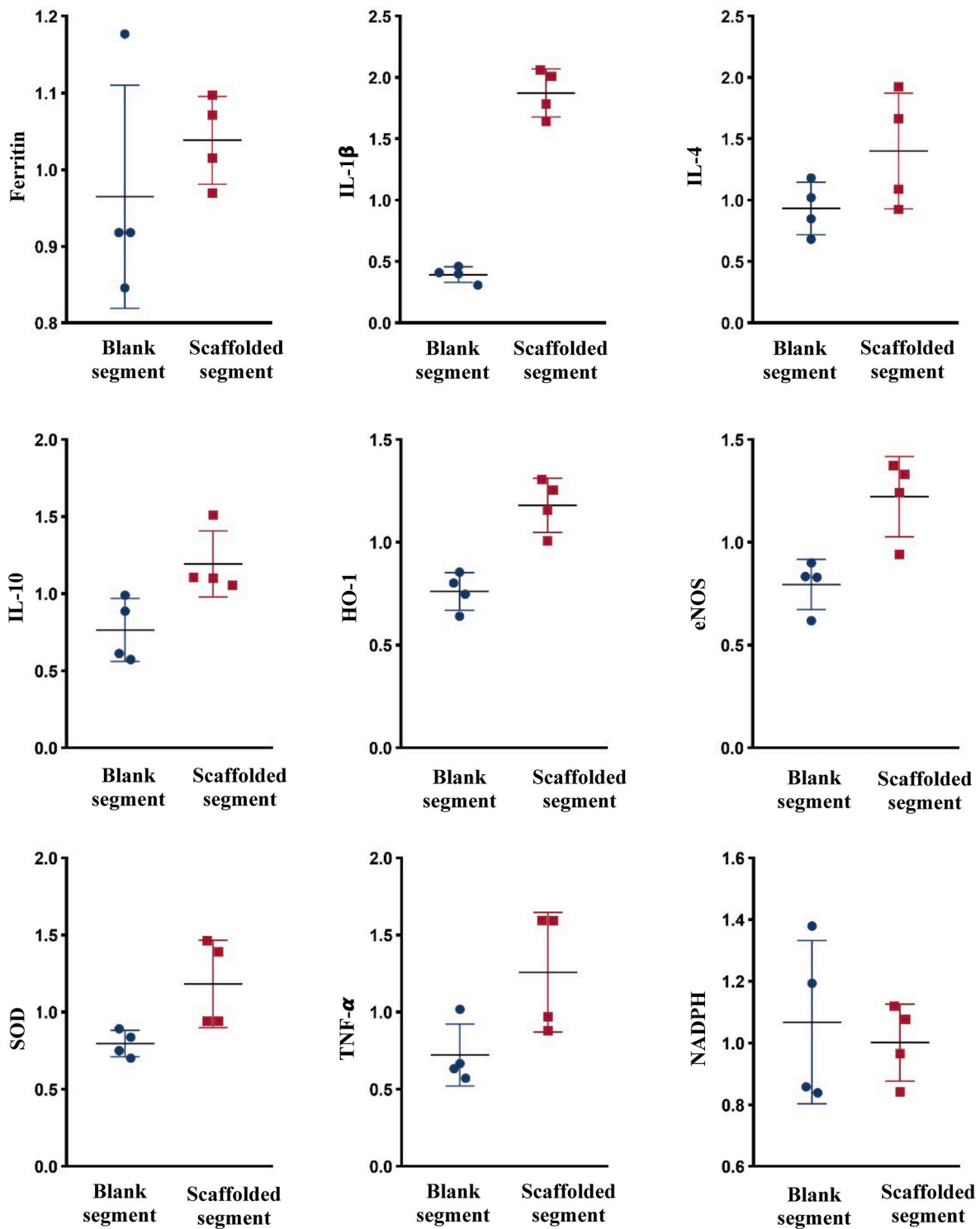
Fig. 7. Comparison of biomarkers by real-time PCR between scaffolded segments and blank segments at 5 years post procedure. eNOS = endothelial nitric oxide synthase; HO = heme oxygenase; IL = interleukin; NADPH = nicotinamide adenine dinucleotide phosphate; PCR = polymerase chain reaction; SOD = superoxide dismutase; TNF = tumor necrosis factor.

Ethics approval and consent to participate

The study protocol was approved by the Institutional Animal Ethics Committee of Fuwai Hospital and confirmed to the ethical standards for medical research involving animal experiments as laid out in the Declaration of Helsinki and its later amendments.

CRediT authorship contribution statement

Ya-Nan Gao: Writing – review & editing, Writing – original draft, Visualization, Investigation, Formal analysis. **Hong-Tao Yang:** Writing – review & editing, Visualization, Investigation. **Zi-Feng Qiu:** Writing – review & editing, Visualization, Investigation, Data curation. **Feng Qi:** Supervision. **Qian-Hong Lu:** Formal analysis, Data curation. **Jian-Feng**
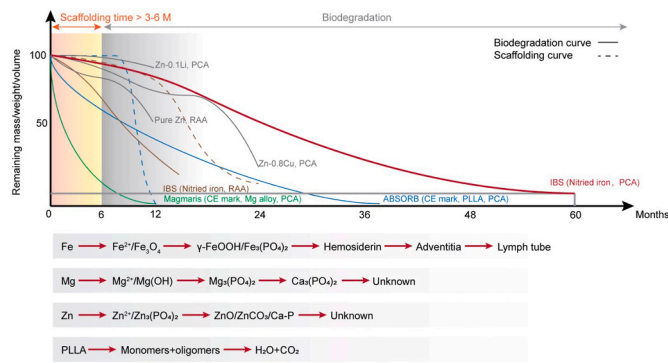
Fig. 8. Degradation behaviors of the representative biodegradable vascular scaffolds and their biodegradation pathways. IBS = sirolimus eluting iron bioresorbable coronary scaffold; PLLA = poly-L-lactic acid.

Zheng: Resources, Project administration, Formal analysis, Data curation. **Zi-Wei Xi:** Visualization, Formal analysis, Data curation. **Xin Wang:** Resources, Investigation. **Li Li:** Visualization, Software, Formal analysis. **Gui Zhang:** Supervision, Project administration, Methodology, Conceptualization. **De-Yuan Zhang:** Validation, Project administration, Investigation, Conceptualization. **Yu-Die Lu:** Supervision, Formal analysis, Data curation. **Hai-Ping Qi:** Writing – review & editing, Supervision. **Hong Qiu:** Writing – review & editing, Supervision, Funding acquisition, Conceptualization. **Run-Lin Gao:** Supervision, Funding acquisition, Conceptualization. **Yu-Feng Zheng:** Supervision.

Declaration of competing interest

H. Qiu and R. L. Gao received institutional research grants from Biotyx Medical (Shenzhen) Co. Ltd., Shenzhen. China. G. Zhang, D. Y. Zhang, H. P. Qi, and Y. D. Lu are employees of Biotyx Medical (Shenzhen) Co. Ltd. Y. F. Zheng is an editor-in-chief for Bioactive Materials and was not involved in the editorial review or the decision to publish this article. All other authors have no relationships relevant to the contents of this paper to disclose.

Acknowledgements

Appendix A. Supplementary data

Supplementary data to this article can be found online at https://doi.org/10.1016/j.bioactmat.2024.05.027.

References

[1] H.Y. Ang, H. Bulluck, P. Wong, S.S. Venkatraman, Y. Huang, N. Foin, Bioresorbable stents: current and upcoming bioresorbable technologies, Int. J. Cardiol. 228 (2017) 931–939.

[2] M. Joner, A.V. Finn, A. Farb, E.K. Mont, F.D. Kolodgie, E. Ladich, R. Kutys, K. Skorija, H.K. Gold, R. Virmani, Pathology of drug-eluting stents in humans: delayed healing and late thrombotic risk, J. Am. Coll. Cardiol. 48 (1) (2006) 193–202.

[3] J. Wiebe, H.M. Nef, C.W. Hamm, Current status of bioresorbable scaffolds in the treatment of coronary artery disease, J. Am. Coll. Cardiol. 64 (23) (2014) 2541–2551.

[4] P.W. Serruys, B. Chevalier, Y. Sotomi, A. Cequier, D. Carrié, J.J. Piek, A.J. Van Boven, M. Dominici, D. Dudek, D. McClean, S. Helqvist, M. Haude, S. Reith, M. de Sousa Almeida, G. Campo, A. Iñiguez, M. Sabaté, S. Windecker, Y. Onuma, Comparison of an everolimus-eluting bioresorbable scaffold with an everolimus-eluting metallic stent for the treatment of coronary artery stenosis (ABSORB II): a 3 year, randomised, controlled, single-blind, multicentre clinical trial, Lancet 388 (10059) (2016) 2479–2491.

[5] Z.A. Ali, P.W. Serruys, T. Kimura, R. Gao, S.G. Ellis, D.J. Kereiakes, Y. Onuma, C. Simonton, Z. Zhang, G.W. Stone, 2-year outcomes with the Absorb bioresorbable scaffold for treatment of coronary artery disease: a systematic review and meta-analysis of seven randomised trials with an individual patient data substudy, Lancet 390 (10096) (2017) 760–772.

[6] M.V. Madhavan, A.J. Kirtane, B. Redfors, P. Généreux, O. Ben-Yehuda, T. Palmerini, U. Benedetto, G. Biondi-Zoccai, P.C. Smits, C. von Birgelen, R. Mehran, T. McAndrew, P.W. Serruys, M.B. Leon, S.J. Pocock, G.W. Stone, Stent-related adverse events >1 Year after Percutaneous coronary intervention, J. Am. Coll. Cardiol. 75 (6) (2020) 590–604.

[7] M. Haude, H. Ince, S. Kische, A. Abizaid, R. Tölg, P. Alves Lemos, N.M. Van Mieghem, S. Verheye, C. von Birgelen, E.H. Christiansen, W. Wijns, H.M. Garcia-Garcia, R. Waksman, Sustained safety and clinical performance of a drug-eluting absorbable metal scaffold up to 24 months: pooled outcomes of BIOSOLVE-II and BIOSOLVE-III, EuroIntervention 13 (4) (2017) 432–439.

[8] M. Haude, H. Ince, A. Abizaid, R. Toelg, P.A. Lemos, C. von Birgelen, E. H. Christiansen, W. Wijns, F.J. Neumann, C. Kaiser, E. Eeckhout, S.T. Lim, J. Escaned, Y. Onuma, H.M. Garcia-Garcia, R. Waksman, Sustained safety and performance of the second-generation drug-eluting absorbable metal scaffold in patients with de novo coronary lesions: 12-month clinical results and angiographic findings of the BIOSOLVE-II first-in-man trial, Eur. Heart J. 37 (35) (2016) 2701–2709.

[9] M. Sabaté, F. Alfonso, A. Cequier, S. Romaní, P. Bordes, A. Serra, A. Iñiguez, P. Salinas, B. García Del Blanco, J. Goicolea, R. Hernández-Antolín, J. Cuesta, J. A. Gómez-Hospital, L. Ortega-Paz, J. Gomez-Lara, S. Brugaletta, Magnesium-based resorbable scaffold versus permanent metallic sirolimus-eluting stent in patients with ST-segment resolution myocardial infarction: the MAGSTEMI randomized clinical trial, Circulation 140 (23) (2019) 1904–1916.

[10] Y. Qi, H. Qi, Y. He, W. Lin, P. Li, L. Qin, Y. Hu, L. Chen, Q. Liu, H. Sun, Q. Liu, G. Zhang, S. Cui, J. Hu, L. Yu, D. Zhang, J. Ding, Strategy of metal-polymer composite stent to accelerate biodegradation of iron-based biomaterials, ACS Appl. Mater. Interfaces 10 (1) (2018) 182–192.

[11] Y. Qi, X. Li, Y. He, D. Zhang, J. Ding, Mechanism of acceleration of iron corrosion by a polylactide coating, ACS Appl. Mater. Interfaces 11 (1) (2019) 202–218.

[12] J. Fu, Y. Su, Y.X. Qin, Y. Zheng, Y. Wang, D. Zhu, Evolution of metallic cardiovascular stent materials: a comparative study among stainless steel, magnesium and zinc, Biomaterials 230 (2020) 119641.

[13] M. Rafaeva, E.R. Horton, A.R.D. Jensen, C.D. Madsen, R. Reuten, O. Willacy, C. B. Brchner, T.H. Jensen, K.W. Zornhagen, M. Crespo, Modeling metastatic colonization in a decellularized organ scaffold-based perfusion bioreactor (adv. Healthcare mater. 1/2022), Adv. Healthcare Mater. 11 (1) (2022).

[14] X. Li, J. Ding, Establishment of coverage-mass equation to quantify the corrosion inhomogeneity and examination of medium effects on iron corrosion, Regen Biomater 10 (2023) rbad007.

[15] H. Zhang, X. Li, Z. Qu, W. Zhang, Q. Wang, D. Cao, Y. Wang, X. Wang, Y. Wang, L. Yu, J. Ding, Effects of serum proteins on corrosion rates and product bioabsorbability of biodegradable metals, Regen Biomater 11 (2024) rbad112.

[16] J.F. Zheng, H. Qiu, Y. Tian, X.Y. Hu, T. Luo, C. Wu, Y. Tian, Y. Tang, L.F. Song, L. Li, L. Xu, B. Xu, R.L. Gao, Preclinical evaluation of a novel sirolimus-eluting iron bioresorbable coronary scaffold in porcine coronary artery at 6 months, JACC Cardiovasc. Interv. 12 (3) (2019) 245–255.

[17] W. Lin, L. Qin, H. Qi, D. Zhang, G. Zhang, R. Gao, H. Qiu, Y. Xia, P. Cao, X. Wang, W. Zheng, Long-term in vivo corrosion behavior, biocompatibility and bioresorption mechanism of a bioresorbable nitrided iron scaffold, Acta Biomater. 54 (2017) 454–468.

[18] B. Medical, The Introduction of the IBS Coronary Scaffold..

[19] F. Otsuka, M. Vorpahl, M. Nakano, J. Foerst, J.B. Newell, K. Sakakura, R. Kutys, E. Ladich, A.V. Finn, F.D. Kolodgie, R. Virmani, Pathology of second-generation everolimus-eluting stents versus first-generation sirolimus- and paclitaxel-eluting stents in humans, Circulation 129 (2) (2014) 211–223.

[20] R. Gao, Y. Yang, Y. Han, Y. Huo, J. Chen, B. Yu, X. Su, L. Li, H.C. Kuo, S.W. Ying, W. F. Cheong, Y. Zhang, X. Su, B. Xu, J.J. Popma, G.W. Stone, Bioresorbable vascular scaffolds versus metallic stents in patients with coronary artery disease: ABSORB China trial, J. Am. Coll. Cardiol. 66 (21) (2015) 2298–2309.

[21] D.J. Kereiakes, S.G. Ellis, C. Metzger, R.P. Caputo, D.G. Rizik, P.S. Teirstein, M. R. Litt, A. Kini, A. Kabour, S.O. Marx, J.J. Popma, R. McGreevy, Z. Zhang, C. Simonton, G.W. Stone, 3-Year clinical outcomes with everolimus-eluting bioresorbable coronary scaffolds: the ABSORB III trial, J. Am. Coll. Cardiol. 70 (23) (2017) 2852–2862.

[22] N. Kukreja, Y. Onuma, P.W. Serruys, Xience V everolimus-eluting coronary stent, Expet Rev. Med. Dev. 6 (3) (2009) 219–229.

[23] C. Wu, H. Qiu, X.Y. Hu, Y.M. Ruan, Y. Tian, Y. Chu, X.L. Xu, L. Xu, Y. Tang, R. L. Gao, Short-term safety and efficacy of the biodegradable iron stent in mini-swine coronary arteries, Chin Med J (Engl) 126 (24) (2013) 4752–4757.

[24] D. Bian, L. Qin, W. Lin, D. Shen, H. Qi, X. Shi, G. Zhang, H. Liu, H. Yang, J. Wang, D. Zhang, Y. Zheng, Magnetic resonance (MR) safety and compatibility of a novel iron bioresorbable scaffold, Bioact. Mater. 5 (2) (2020) 260–274.

[25] W. Lin, H. Zhang, W. Zhang, H. Qi, G. Zhang, J. Qian, X. Li, L. Qin, H. Li, X. Wang, H. Qiu, X. Shi, W. Zheng, D. Zhang, R. Gao, J. Ding, In vivo degradation and endothelialization of an iron bioresorbable scaffold, Bioact. Mater. 6 (4) (2021) 1028–1039.

[26] P. Rippstein, M.K. Black, M. Boivin, J.P. Veinot, X. Ma, Y.X. Chen, P. Human, P. Zilla, E.R. O'Brien, Comparison of processing and sectioning methodologies for arteries containing metallic stents, J. Histochem. Cytochem. 54 (6) (2006) 673–681.

[27] P.W. Serruys, Y. Katagiri, Y. Sotomi, Y. Zeng, B. Chevalier, R.J. van der Schaaf, A. Baumbach, P. Smits, N.M. van Mieghem, A. Bartorelli, P. Barragan, A. Gershlick, R. Kornowski, C. Macaya, J. Ormiston, J. Hill, I.M. Lang, M. Egred, J. Fajadet, M. Lesiak, S. Windecker, R.A. Byrne, L. Räber, R.J. van Geuns, G.S. Mintz, Y. Onuma, Arterial remodeling after bioresorbable scaffolds and metallic stents, J. Am. Coll. Cardiol. 70 (1) (2017) 60–74.

[28] J. Ma, N. Zhao, L. Betts, D. Zhu, Bio-adaption between magnesium alloy stent and the blood vessel: a review, J. Mater. Sci. Technol. 32 (9) (2016) 815–826.

[29] F. Otsuka, E. Pacheco, L.E. Perkins, J.P. Lane, Q. Wang, M. Kamberi, M. Frie, J. Wang, K. Sakakura, K. Yahagi, E. Ladich, R.J. Rapoza, F.D. Kolodgie, R. Virmani, Long-term safety of an everolimus-eluting bioresorbable vascular scaffold and the cobalt-chromium XIENCE V stent in a porcine coronary artery model, Circ Cardiovasc Interv 7 (3) (2014) 330–342.

[30] Y. Onuma, D. Dudek, L. Thuesen, M. Webster, K. Nieman, H.M. Garcia-Garcia, J. A. Ormiston, P.W. Serruys, Five-year clinical and functional multislice computed tomography angiographic results after coronary implantation of the fully resorbable polymeric everolimus-eluting scaffold in patients with de novo coronary artery disease: the ABSORB cohort A trial, JACC Cardiovasc. Interv. 6 (10) (2013) 999–1009.

[31] J.A. Ormiston, P.W. Serruys, E. Regar, D. Dudek, L. Thuesen, M.W. Webster, Y. Onuma, H.M. Garcia-Garcia, R. McGreevy, S. Veldhof, A bioabsorbable everolimus-eluting coronary stent system for patients with single de-novo coronary artery lesions (ABSORB): a prospective open-label trial, Lancet 371 (9616) (2008) 899–907.

[32] P.W. Serruys, J.A. Ormiston, Y. Onuma, E. Regar, N. Gonzalo, H.M. Garcia-Garcia, K. Nieman, N. Bruining, C. Dorange, K. Miquel-Hébert, S. Veldhof, M. Webster, L. Thuesen, D. Dudek, A bioabsorbable everolimus-eluting coronary stent system (ABSORB): 2-year outcomes and results from multiple imaging methods, Lancet 373 (9667) (2009) 897–910.

[33] R. Erbel, C. Di Mario, J. Bartunek, J. Bonnier, B. de Bruyne, F.R. Eberli, P. Erne, M. Haude, B. Heublein, M. Horrigan, C. Ilsley, D. Böse, J. Koolen, T.F. Lüscher, N. Weissman, R. Waksman, Temporary scaffolding of coronary arteries with bioabsorbable magnesium stents: a prospective, non-randomised multicentre trial, Lancet 369 (9576) (2007) 1869–1875.

[34] M. Madhavan, A. Kirtane, B. Redfors, P. Généreux, P. Smits, R. Mehran, R. Parvataneni, G. Stone, TCT-313 incidence and predictors of very late major adverse cardiac events after metallic stents: a patient-level pooled analysis from seventeen randomized trials, J. Am. Coll. Cardiol. 68 (18) (2016) B129–B130.

[35] A. El Ayadi, J.W. Jay, A. Prasai, Current approaches targeting the wound healing phases to attenuate fibrosis and scarring, Int. J. Mol. Sci. 21 (3) (2020).

[36] G.C. Gurtner, S. Werner, Y. Barrandon, M.T. Longaker, Wound repair and regeneration, Nature 453 (7193) (2008) 314–321.

[37] Y. Nuki, M.M. Matsumoto, E. Tsang, W.L. Young, N. van Rooijen, C. Kurihara, T. Hashimoto, Roles of macrophages in flow-induced outward vascular remodeling, J. Cerebr. Blood Flow Metabol. 29 (3) (2009) 495–503.

[38] F. Tronc, Z. Mallat, S. Lehoux, M. Wassef, B. Esposito, A. Tedgui, Role of matrix metalloproteinases in blood flow-induced arterial enlargement: interaction with NO, Arterioscler. Thromb. Vasc. Biol. 20 (12) (2000) E120–E126.

[39] R.H. Cox, Arterial wall mechanics and composition and the effects of smooth muscle activation, Am. J. Physiol. 229 (3) (1975) 807–812.

[40] W.A. Omar, D.J. Kumbhani, The current literature on bioabsorbable stents: a review, Curr. Atherosclerosis Rep. 21 (12) (2019) 54.

[41] D. Shen, H. Qi, W. Lin, W. Zhang, D. Bian, X. Shi, L. Qin, G. Zhang, W. Fu, K. Dou, B. Xu, Z. Yin, J. Rao, M. Alwi, S. Wang, Y. Zheng, D. Zhang, R. Gao, PDLLA-Zn-nitrided Fe bioresorbable scaffold with 53-μm-thick metallic struts and tunable multistage biodegradation function, Sci. Adv. 7 (23) (2021).

[42] Y. Onuma, P.W. Serruys, L.E. Perkins, T. Okamura, N. Gonzalo, H.M. García-García, E. Regar, M. Kamberi, J.C. Powers, R. Rapoza, Intracoronary optical coherence tomography and histology at 1 month and 2, 3, and 4 years after implantation of everolimus-eluting bioresorbable vascular scaffolds in a porcine coronary artery model an attempt to decipher the human optical coherence tomography images in the ABSORB trial, Circulation 122 (22) (2010) 2288–2300.

[43] D.J. Kereiakes, Y. Onuma, P.W. Serruys, G.W. Stone, Bioresorbable vascular scaffolds for coronary revascularization, Circulation 134 (2) (2016) 168–182.

[44] G. Caiazzo, I.D. Kilic, E. Fabris, R. Serdoz, A. Mattesini, N. Foin, S. De Rosa, C. Indolfi, C. Di Mario, Absorb bioresorbable vascular scaffold: what have we learned after 5 years of clinical experience? Int. J. Cardiol. 201 (2015) 129–136.

[45] P. Poncin, C. Millet, J. Chevy, J. Proft, Comparing and optimizing Co-Cr tubing for stent applications. Proceedings of the Materials and Processes for Medical Devices Conference, 2004, pp. 279–283.

[46] R. Waksman, R. Erbel, C. Di Mario, J. Bartunek, B. de Bruyne, F.R. Eberli, P. Erne, M. Haude, M. Horrigan, C. Ilsley, Early-and long-term intravascular ultrasound and angiographic findings after bioabsorbable magnesium stent implantation in human coronary arteries, JACC Cardiovasc. Interv. 2 (4) (2009) 312–320.

[47] E. Wittchow, N. Adden, J. Riedmüller, C. Savard, R. Waksman, M. Braune, Bioresorbable drug-eluting magnesium-alloy scaffold: design and feasibility in a porcine coronary model, EuroIntervention 8 (12) (2013) 1441–1450.

[48] M. Haude, R. Erbel, P. Erne, S. Verheye, H. Degen, D. Böse, P. Vermeersch, I. Wijnbergen, N. Weissman, F. Prati, Safety and performance of the drug-eluting absorbable metal scaffold (DREAMS) in patients with de-novo coronary lesions: 12 month results of the prospective, multicentre, first-in-man BIOSOLVE-I trial, Lancet 381 (9869) (2013) 836–844.

[49] M. Haude, H. Ince, A. Abizaid, R. Toelg, P.A. Lemos, C. von Birgelen, E. H. Christiansen, W. Wijns, F.-J. Neumann, C. Kaiser, Safety and performance of the second-generation drug-eluting absorbable metal scaffold in patients with de-novo coronary artery lesions (BIOSOLVE-II): 6 month results of a prospective, multicentre, non-randomised, first-in-man trial, Lancet 387 (10013) (2016) 31–39.

[50] J. Bennett, Q. De Hemptinne, K. McCutcheon, Magmaris resorbable magnesium scaffold for the treatment of coronary heart disease: overview of its safety and efficacy, Expet Rev. Med. Dev. 16 (9) (2019) 757–769.

[51] H. Yang, C. Wang, C. Liu, H. Chen, Y. Wu, J. Han, Z. Jia, W. Lin, D. Zhang, W. Li, Evolution of the degradation mechanism of pure zinc stent in the one-year study of rabbit abdominal aorta model, Biomaterials 145 (2017) 92–105.

[52] C. Zhou, H.F. Li, Y.X. Yin, Z.Z. Shi, H.J. Zhang, Long-term in vivo study of biodegradable Zn-Cu stent: a 2-year implantation evaluation in porcine coronary artery, Acta Biomater. 97 (2019).

[53] H. Yang, D. Jin, J. Rao, J. Shi, G. Li, C. Wang, K. Yan, J. Bai, G. Bao, M. Yin, Lithium-Induced optimization mechanism for an ultrathin-strut biodegradable Zn-based vascular scaffold, Adv. Mater. (2023) 2301074.

[54] M. Peuster, P. Wohlsein, M. Brügmann, M. Ehlerding, K. Seidler, C. Fink, H. Brauer, A. Fischer, G. Hausdorf, A novel approach to temporary stenting: degradable cardiovascular stents produced from corrodible metal-results 6-18 months after implantation into New Zealand white rabbits, Heart 86 (5) (2001) 563–569.

[55] D. Zhang, Z. Cai, N. Liao, S. Lan, M. Wu, H. Sun, Z. Wei, J. Li, X. Liu, pH/hypoxia programmable triggered cancer photo-chemotherapy based on a semiconducting polymer dot hybridized mesoporous silica framework, Chem. Sci. 9 (37) (2018) 7390–7399.

[56] S.T. Chou, M. Alsawas, R.M. Fasano, J.J. Field, J.E. Hendrickson, J. Howard, M. Kameka, J.L. Kwiatkowski, F. Pirenne, P.A. Shi, S.R. Stowell, S.L. Thein, C. M. Westhoff, T.E. Wong, E.A. Akl, American Society of Hematology 2020 guidelines for sickle cell disease: transfusion support, Blood Adv 4 (2) (2020) 327–355.

[57] D. Qiu, Y. Deng, Y. Wen, J. Yin, J. Feng, J. Huang, M. Song, G. Zhang, C. Chen, J. Xia, Iron corroded granules inhibiting vascular smooth muscle cell proliferation, Mater Today Bio 16 (2022) 100420.

[58] M. Peuster, C. Hesse, T. Schloo, C. Fink, P. Beerbaum, C. von Schnakenburg, Long-term biocompatibility of a corrodible peripheral iron stent in the porcine descending aorta, Biomaterials 27 (28) (2006) 4955–4962.

[59] R.L. Gao, B. Xu, Z. Sun, C. Guan, L. Song, L. Gao, C. Li, J. Cui, Y. Zhang, K. Dou, J. Chen, C. Mu, H. Liu, A. Li, Z. Li, L. Xie, Y. Yang, S. Qiao, Y. Wu, G.W. Stone, First-in-human evaluation of a novel ultrathin sirolimus-eluting iron bioresorbable scaffold: 3-year outcomes of the IBS-FIM trial, EuroIntervention 19 (3) (2023) 222–231.